

Transport Phenomena in the Edge of Alcator C-Mod Plasmas

J.L. Terry 1), N.P. Basse 1), I. Cziegler 1), M. Greenwald 1), O. Grulke 2), B. LaBombard 1), S.J. Zweben 3), E.M. Edlund 1), J.W. Hughes 1), L. Lin 1), Y. Lin 1), M. Porkolab 1), M. Sampsell 4), B. Veto 1), S.J. Wukitch 1)

1) Plasma Science and Fusion Center, MIT, Cambridge, MA 02139-4307

2) MPI for Plasma Physics, EURATOM Association and Ernst-Moritz-Arndt University Greifswald, Germany

3) Princeton Plasma Physics Laboratory, Princeton, NJ 08543, USA

4) Fusion Research Center, The University of Texas at Austin, Austin, TX 78712, USA

e-mail contact of main author: terry@psfc.mit.edu

Abstract. Two aspects of edge turbulence and transport in Alcator C-Mod are explored. The quasi-coherent mode, an edge fluctuation present in Enhanced D \square H-mode plasmas, is examined with regard to its role in the enhanced particle transport found in these plasmas, its in/out asymmetry, its poloidal wave number, and its radial width and location. It is shown to play a dominant role in the perpendicular particle transport. The QCM is not observed at the inboard midplane, indicating that its amplitude there is significantly smaller than on the outboard side. The peak amplitude of the QCM is found just inside the separatrix, with a radial width ≥ 5 mm, leading to a non-zero amplitude outside the separatrix and qualitatively consistent with its transport enhancement. Also examined are the characteristics of the intermittent convective transport, associated with “blobs” and typically occurring in the scrape-off-layer. The blobs are qualitatively similar in L- and H-mode. When their sizes, occurrence frequencies, and magnitudes are compared, it is found that the blob size may be somewhat smaller in ELMfree H-Mode, and blob frequency is similar. A clear difference is seen in the blob magnitude in the far SOL, with ELMfree H-mode showing a smaller perturbation there than L-mode. As the Greenwald density limit is approached ($n/n_{GW} \geq 0.7$), blobs are seen inside the separatrix, consistent with the observation that the high cross-field transport region, normally found in the far scrape-off, penetrates the closed flux surfaces at high n/n_{GW} .

1. Introduction

Transport in the edge and scrape-off-layer (SOL) can play a crucial role in overall plasma confinement, for example through the formation and character of the H-mode edge transport barrier or as a key aspect of the density limit [1]. The research described here concentrates on two phenomena observed in the edge and SOL of Alcator C-Mod plasmas, both involved with cross-field particle transport. The first phenomenon is the Quasi-Coherent Mode fluctuation that is observed in Enhanced-D \square (EDA) H-mode plasmas, while the second is the intermittent turbulence [2], often identified as blobs, typically associated with the far SOL and enhanced main chamber recycling. In the case of the QCM, after showing evidence that it is largely responsible for the enhanced particle transport in EDA H-mode, we will address the inboard-outboard asymmetry of its magnitude, its radial width and location at the outboard midplane, and its poloidal wave number. The importance of the intermittent blob transport derives from the fact that the cross-field particle fluxes it drives can be greater than the parallel fluxes [3], with significant implications for recycling and divertor design. It has also been implicated as playing an important role in the density limit [1]. We will discuss the in/out asymmetry of the broadband fluctuations dominated by the blobs, as well as characterize the similarities and differences of the blob turbulence in C-Mod’s L- and H-mode plasmas. Finally we will present observations of blobs being generated *inside* the separatrix as the density limit is

approached, thereby supporting the hypothesis that the penetration of blob transport into the closed flux surfaces may be related to the density limit.

2. Experimental Diagnostics

The primary diagnostics used to characterize the two edge phenomena of interest here are the optical “gas-puff-imaging” (GPI) diagnostics, the phase-contrast-imaging (PCI) diagnostic, and scanning Langmuir probes. While the QCM is readily observable by a number of other diagnostics, e.g. reflectometry, BES, magnetic pick-up coils mounted in a scanning probe head, we discuss characteristics of the mode as measured by the GPI optical diagnostics and PCI. In determining characteristics of the blob turbulence, we use measurements from the GPI and the scanning Langmuir probes.

GPI [4,5,6] was developed in order to study edge turbulence. With this technique, emission is localized in the toroidal dimension, thereby overcoming a disadvantage of line-of-sight-integrating, passive optical diagnostics. With GPI, emission (D_{\square} or HeI) from a localized gas puff is made to be much greater (typically $\geq 5x$) than any intrinsic emission along the line-of-sight. Since the gas puff emission is viewed along the sight lines that are configured to cross it, spatial localization is provided. In C-Mod gas-puff barrels are located on both inboard and outboard sides, near the plasma midplane and typically only 1-3 cm from the separatrix. The outboard gas puff is viewed by two arrays, one made up of discrete fibers whose focal spots are arranged in a radial array in front of the barrel. The focal spots are typically 4-5 mm in diameter and together span the plasma edge. The fibers transmit light to photodiodes filtered for D_{\square} and having flat frequency response for frequencies ≥ 250 kHz. A coherent fiber bundle is also employed to image in 2D the emission in front of the outboard barrel. Its view is parallel to the magnetic field at the gas puff location and thus images the structure of the emission perpendicular to the field. The 2D image is transmitted to a 300 frame movie camera with a maximum frame rate of 250 kHz. The camera’s 64x64 pixel array, in combination with the imaging optics, yield ~ 2 mm spatial resolution in the plasma [7]. Both of these GPI systems detect the QCM and the blobs. The inboard gas-puff is viewed by another radially-resolving array of fibers. These array-views span the inboard separatrix and are used for comparing with observations from the outboard side.

3. Characteristics of the Quasi-Coherent Mode

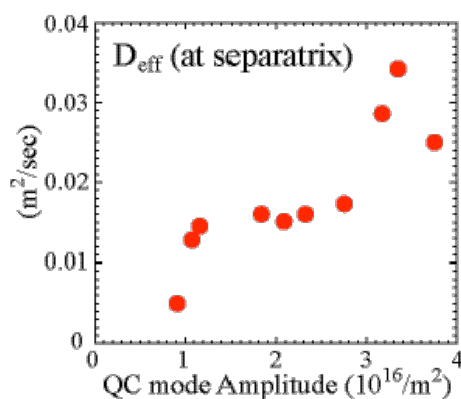


FIG. 1 Increase of D_{eff} with the increase of the QCM amplitude.

EDA H-mode confinement in C-Mod is distinguished by good energy confinement, but with enough particle transport that the density does not increase monotonically and the impurities do not accumulate, as occurs in ELMfree H-mode. The enhanced particle transport appears to be provided by the QCM, a fluctuation that is localized to the edge pedestal region. The QCM is a fluctuation of density, potential, and magnetic field [8], with a frequency spectrum peaked typically between 90 and 200 kHz. The evidence that the QCM is responsible for the enhanced transport is 1) the magnitude of the oscillation is observed to be

proportional to the time-averaged “effective particle diffusion coefficient”, D_{eff} (defined below), and 2) the absence of the fluctuation in ELM-free H-modes, in which both density and impurities accumulate. The first statement is illustrated in Fig. 1, where $D_{\text{eff}} = -\dot{\rho}_{\text{perp}}/\dot{\rho}_{\text{ne}}$,

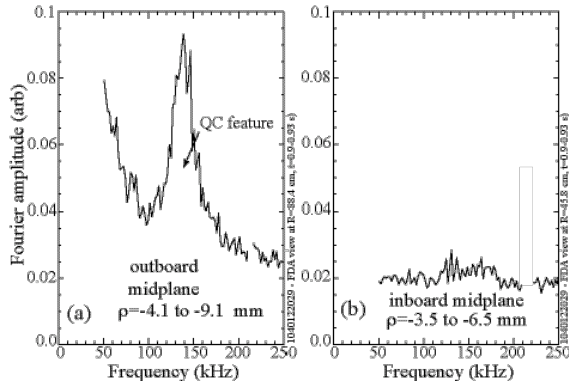


FIG. 2(a) QCM feature as observed on a single outboard view; such a feature is seen on views spanning $-13 < \rho < 3$ mm (spot sizes ~ 5 mm). (b) Same spectral region (at the same time) for fluctuations from a single inboard midplane view. No feature is seen for $-6.5 < \rho < 5$ mm.

pedestal, we have investigated a number of its characteristics. The first is its poloidal character. It is known that the QCM is localized to the edge pedestal region, at least on the outboard side, as documented by probes [10,11], BES [12] and reflectometry. In addition, the PCI measurements of the mode are consistent with its existence in the pedestal at the *top* and *bottom* of the plasma at major radii near the plasma center, but still outboard of the X-point. The outboard GPI arrays also detect the QCM since its density fluctuation is manifested as an emission fluctuation. An example of the frequency spectrum of GPI emission from 50 to 250 kHz is shown in Fig. 2a. The emission is detected by one of the radial array views, viewing the puff at $\rho \sim -7$ mm, i.e. ~ 7 mm inside the separatrix. (ρ is the radial distance beyond the separatrix of a given point when flux-surface-mapped to the outside midplane.) In contrast, there is no evidence of the QCM feature at the *inboard* midplane, even at inboard locations that are on flux surfaces that exhibit the fluctuation on the outboard side. The absence of an inboard QCM feature is evident in Fig. 2b, where a spectrum from one of the inboard views is shown. Thus we conclude that the QCM mode amplitude is much reduced at the inboard midplane, implying that curvature is involved in the drive for this mode.

Using the 2D view of the GPI camera, we can examine the radial structure and poloidal wave number of the mode at the outboard midplane. With the camera’s 250 kHz frame rate, frequencies up to 125 kHz are measurable without aliasing. The camera’s view is such that it is sensitive to fluctuations with poloidal wave number in the range $0.4 \text{ cm}^{-1} < |k_{\perp}| < 15 \text{ cm}^{-1}$ (limited by the ~ 8 cm vertical extent of the view on the low side and by the ~ 0.2 cm camera resolution on the high side). The QCM is much more difficult to detect with the camera than it is using the outboard diode array (which samples at 1 MHz for ~ 125 ms). In fact, the frequency spectra from individual camera pixels (with relatively noisy 300-point time-series signals) show no clear QCM feature above the noise. In order to overcome this limitation we utilized the 2D, many-pixel feature of the camera images and the fact that the mode is field-aligned [8]. By averaging the (complex) frequency Fourier coefficients from those pixels viewing the same flux surface and by performing that average at different k_{\perp}

is plotted versus the QCM amplitude. D_{eff} is determined from probe measurements of $\dot{\rho}_{\text{ne}}$, with $\dot{\rho}_{\text{perp}}$ inferred [9] from spatially-resolved measurements of the ionization source, including the effects of parallel plasma flows toward the divertor. (Note that the use of D_{eff} is not meant to imply that the transport is wholly or even primarily diffusive.) The QCM amplitude is measured by the PCI diagnostic which measures line integrated density fluctuations along 12 vertical chords that together span a ~ 4 cm section of radial width, crossing the midplane near the plasma center [8].

Because of the primary role of the QCM in the particle transport out of the

values, the QCM amplitude on the specific flux surface emerges from the noise. Spectra determined this way and showing the k_{\perp}, f dependence are shown in Fig. 3a. In this case, the fluctuation is seen to have a frequency of ~ 100 kHz and a k_{\perp} of ~ 1.0 cm^{-1} . $k_{\perp} > 0$ indicates a wave propagating in the electron diamagnetic direction (up in the camera's view). The frequency of the feature is the same as that measured simultaneously by the PCI (Fig. 3b) and by the outboard diode array. Fig. 3b shows the (f, k_R) spectrum¹ of density fluctuations as measured by the PCI. The two features at $k_R \sim -4$ cm^{-1} and ~ 5.5 cm^{-1} are evidence of the QCM fluctuation propagating in the electron diamagnetic direction at the edge and intersecting the PCI laser beam at the top (thus generating a $k_R < 0$) and at bottom (with $k_R > 0$) of the plasma. (For a schematic of the PCI chords and QCM relative to the plasma, see Fig. 2 in Ref. [8]).

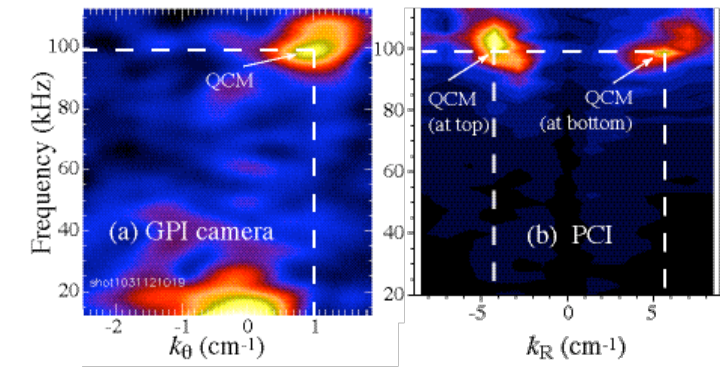


FIG. 3. (a) QCM feature in GPI camera's (f, k_{\perp}) spectrum measured along that fraction of the flux surface in the field-of-view having $\Delta r \sim 10$ mm. (b) QCM feature in (f, k_R) space as detected by the PCI at the same time. Color scales are linear in Fourier amplitude.

These three measurements of wave number are approximately consistent with a field-aligned mode, $\mathbf{k} \cdot \mathbf{B} = 0$, in which case k_{\perp} varies on a flux surface as $k_{\perp}(\square_1) = k_{\perp}(\square_2) [(B_{\perp}(\square_2)/B_{\perp}(\square_1))] \times (R_2/R_1)^2$. Values of -3.7 and 4.3 cm^{-1} are predicted for k_R at the top and bottom PCI locations for a midplane $k_{\perp} = 1 \text{ cm}^{-1}$, the value measured by the GPI. Measurements of k_{\perp} by a probe (located ~ 10 cm above the midplane) [10,11] and measurements of the poloidal variation of k_{\perp} using BES and PCI [12] have been done previously. They also show that k_{\perp} typically varies between 0.8 and 2 cm^{-1} near the outboard midplane and that the poloidal variation is approximately consistent with a field-aligned mode.

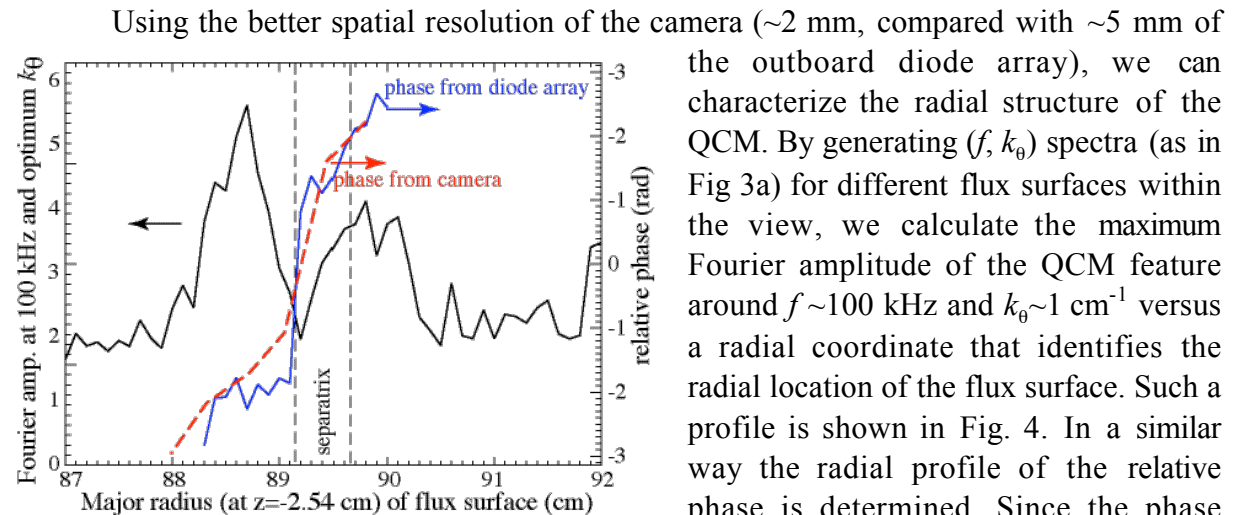


FIG. 4. (black) Radial profile of the QCM amplitude vs. radial location of flux surface. Relative phase as determined by the GPI camera (red dashed) and by the radial diode array (blue). The blue curve has been shifted out by 3mm.

Using the better spatial resolution of the camera (~ 2 mm, compared with ~ 5 mm of the outboard diode array), we can characterize the radial structure of the QCM. By generating (f, k_{\perp}) spectra (as in Fig 3a) for different flux surfaces within the view, we calculate the maximum Fourier amplitude of the QCM feature around $f \sim 100$ kHz and $k_{\perp} \sim 1$ cm^{-1} versus a radial coordinate that identifies the radial location of the flux surface. Such a profile is shown in Fig. 4. In a similar way the radial profile of the relative phase is determined. Since the phase measurement from the camera is relatively uncertain (due to noisier data), we plot it together with that determined using diode array, whose signal-to-noise

¹ Note that the PCI measures k_R , and $|k_R| = |k_{\perp}| / \sin \alpha$, where α is the angle between the separatrix and vertical at the locations where the PCI chords cross the plasma edge.

is greater, but whose resolution is poorer. As shown, agreement is good. While the phase clearly varies radially, the interpretation of this phase variation is still under consideration. The observed radial width is significantly larger than the resolution of the camera. There appear to be two features, a larger peak of ~ 0.5 cm width (FWHM) which is radially inside of a smaller peak of similar width. We note that the outboard diode array yields a radial profile for the mode amplitude that is consistent with that from the camera (Fig. 4), albeit with poorer resolution. We also point out that, while BES [12] and simulations with the BOUT turbulence code [8] yield a similar radial width of ≥ 5 mm, measurements of the width from the scanning probe and from reflectometry yield values ~ 2 mm. The reasons for this difference are still unknown.

Also shown in Fig. 4 is the location of the separatrix, illustrated as a stripe as a result of uncertainties in the registration of the field-of-view (~ 5 mm), as well as uncertainties due to the EFIT reconstruction (~ 2 mm). Even with these uncertainties, it is likely that the mode spans the separatrix. We note that the width of the density pedestal is typically only 2-6 mm [13]. Thus we see that the extension of the QCM onto open field lines is qualitatively consistent with the observation that the QCM strongly affects particle transport (Fig. 1).

4. Comparisons of SOL “blob” turbulence in L- and H-Mode plasmas

We now consider a different aspect of turbulent transport in the edge. This is the intermittent, cross-field transport associated with the radial and poloidal propagation of turbulent structures and shown to dominate the total cross-field transport in the SOL [14]. On C-

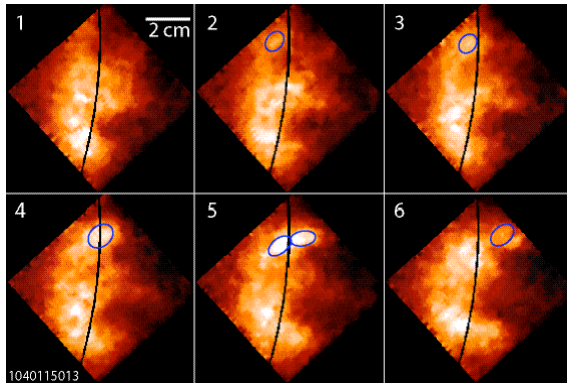


Fig. 5. Movie frames of edge turbulence at $n/n_{GW}=0.8$. The blue ovals locate the “birth” and motion of a blob. The separatrix is also shown. The emission is HeI, and the time between frames is 4 μ sec.

Mod it is studied using probes and GPI. Although the turbulent structures are aligned with the local field, have small k_{\parallel} , and are actually filaments, they have the appearance of “blobs” when viewed along the field. As an example of the “birth” and propagation of a blob, we show six consecutive frames from the GPI camera in Fig 5. Although the birth location of the prominent blob identified in these frames is atypical (and will be discussed in the next section), the blob’s size and its outward propagation are typical. The blobs are detected

as large amplitude events on the signals of the diode array views and as large amplitude ion-saturation-current and floating-potential events by probes. An example of the GPI emission

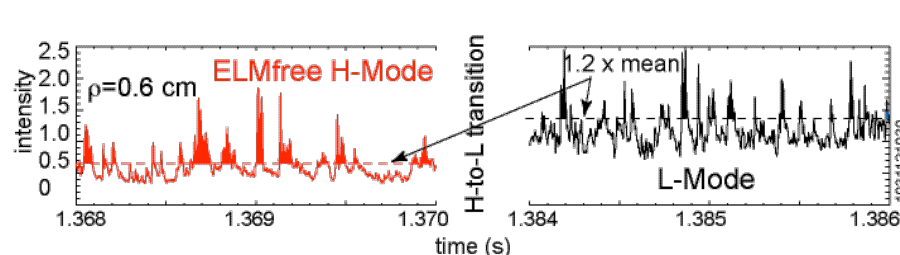


Fig. 6. Time history of GPI emission from an outboard view at $\rho=0.6$ cm (far SOL), during an H-mode period (left) and during the L-mode period (right) following the H-to-L back transition.

time history from one of the outboard views is shown in Fig. 6. In the far SOL the “event” probability distribution function is typically strongly skewed toward larger amplitude events;

both skewness and kurtosis are >0 . It is important to note that both the GPI diagnostics and the probes show that this turbulence is much reduced ($\sim x5$) on the inboard side compared to the outboard side [15], evidence of its probable ballooning character.

We now turn to a comparison of the SOL blob turbulence in L- and H-mode. Similar studies using probes have been reported in Refs. [1,14,16]. Fig. 6 shows the local emission signal first during an ELMfree period and then during a following L-mode period. The time histories indicate that the nature of the blob turbulence is qualitatively similar in L- and H-mode. Using the outboard GPI diagnostics we will compare quantitatively the spatial size of the blob structures, and the frequency and magnitude of the blob events, as well as discuss observations about their radial propagation velocity. In these comparisons we examine the H-mode after the pedestal has developed and the core density has increased significantly, i.e. not immediately after an L-to-H transition when the GPI diagnostics indicate that the SOL is more quiescent. A measure of the spatial size of the blobs is found from the poloidal correlation lengths of the GPI camera images, shown in Fig. 7a. The poloidal and radial correlation lengths are similar [6]. As shown, correlation lengths of the blobs in the far SOL are somewhat smaller in ELMfree H-mode compared to L-mode, although the difference is just within the measurement uncertainty. The frequency of the blob events has been determined using the signals from the outboard diode array. In the analysis it is assumed that as the blobs sweep past the views and are thus detected as emission spikes above what would be expected from random Gaussian-distributed fluctuations. The frequency of distinguishable events above a threshold is calculated (with the threshold set relative to the mean value of the signal). As illustrated in Fig. 6, this amounts to counting the number of time-series local maxima that are above the threshold. In the case where the threshold is 1.2 times the mean, the frequencies are plotted versus ρ in Fig. 7b and are seen to be similar for L-Mode and ELMfree H-mode. This

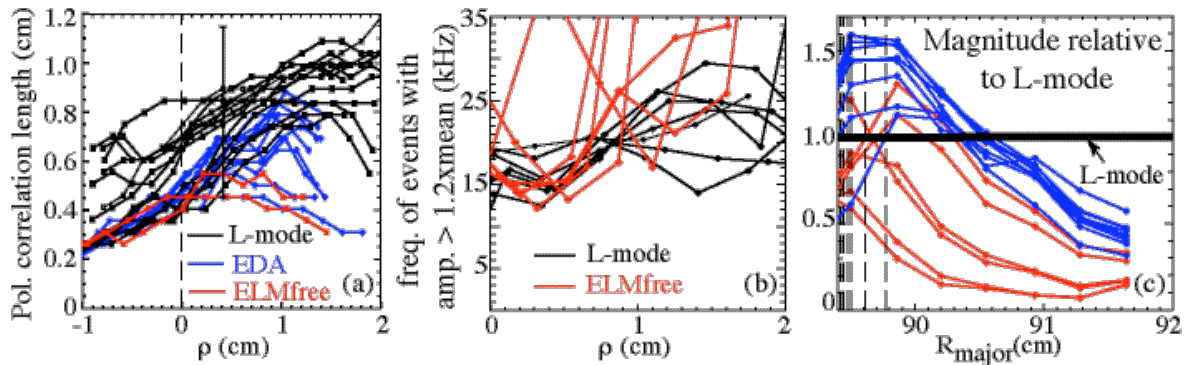


Fig. 7. Comparisons of (a) blob size (poloidal correlation length), (b) blob frequency, and (c) blob magnitude vs. radius. In (c) abssisa values are the major radii for the views and the dashed lines are the separatrix locations during the measurement times.

result depends somewhat on the chosen threshold, since the mean value in H-mode is smaller than in L-mode. We conclude, however, that the frequency of blob events with magnitudes greater than this threshold is similar in the two cases. The *magnitudes* of blob events are compared by examining the integral under those events whose maxima are greater than the threshold, i.e. the sum of the shaded portions in Fig.6. (Note that only the portion above the mean is included in the integral). Since in this case we are comparing intensities (and the diode array views are not absolutely calibrated), we compare the magnitudes relative to L-mode for each view separately. This comparison is shown in Fig. 7c, for which the threshold is also 1.2 times the mean. Here we see a distinct separation between L- and H-mode, with significantly

smaller blob magnitudes in the far SOL during ELMfree H-mode as compared to L-mode. The EDA/L-mode comparison shows an intermediate effect.

The fluctuation phase velocities can also be compared using a time-delay cross-correlation analysis of the GPI camera images [17]. The velocity fields, which are calculated as time averages over the 1.2 ms of camera data, typically show a mixture of radially outward and poloidal motion outside the separatrix. In the SOL the fluctuations are dominated by blobs, so we assume that the fluctuation phase velocity fields reflect the actual motion of the blobs. In lower single null discharges the dominant poloidal direction is downward toward the divertor (ion diamagnetic drift direction). The magnitudes of the radial and poloidal components vary between ~ 0 and 1000 m/s. To date we have not found a systematic difference in velocity fields between L- and H-mode. This is primarily because of a wide variation in SOL velocity fields observed for L-mode discharges.

5. “Blob” turbulence near the density limit

Of particular interest is the generation of the blobs in plasmas near the Greenwald density limit. For discharges away from the limit, the typical event distributions around the separatrix and in the near SOL (both from the probe measurements and the optical measurements) are more gaussian, less skewed toward larger events (i.e. fewer blobs) than is the case in the far SOL [1]. The 2D camera images, which typically show blob generation only outside the separatrix for discharges with $n/n_{GW} < 0.6$, are consistent with this. However, as the density limit is approached, the region of intermittent blob transport expands inward radially, eventually crossing into the closed flux surfaces. Not coincidentally, when that occurs, the

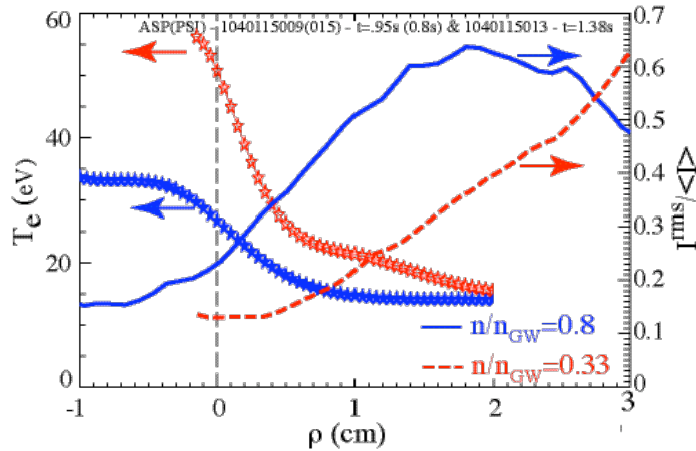


FIG. 8. Radial profiles of T_e and normalized emission fluctuations, I^{RMS}/I_{ave} , at two values of n/n_{GW} , 0.33 (red) and 0.8 (blue). The emission fluctuations are in HeI. Near the density limit, blobs are seen inside the separatrix (Fig. 5).

radial profile of normalized GPI emission fluctuations and the associated T_e profiles at two values of normalized density, $n/n_{GW} = 0.33$ and 0.8. For the case near the density limit, fluctuation levels in the $-1 < \rho < 2$ cm region have increased significantly, while T_e and the temperature gradient at the separatrix have decreased. A larger temperature gradient must exist further inside of $\rho = -1$ cm in order to connect to core T_e profiles. Whereas blobs are typically seen only outside the separatrix, *near the density limit, under these conditions, blob generation*

levels of cross-field convected power are seen to be larger than the power conducted to the divertor, and separatrix temperatures and temperature gradients are reduced [1]. The observations of blob generation inside the separatrix, as illustrated in Fig. 5, add further support to this picture. Although it is hard to quantify the spatial distribution of the blob “birth” locations, we do observe, as is pointed out in Ref. [1], the inward expansion of the region of higher fluctuation levels as the limit is approached. In Fig. 8 is shown the

inside the separatrix is observed (Fig. 5). This is indicative that blob generation is associated with gradients rather than with the transition from closed to open field lines.

6. Discussion

The origin of the QCM is still unknown. Nonetheless it has been shown to be important in providing the beneficial particle transport that flushes impurities and the opportunity for density control. The in/out asymmetry in its amplitude provides a clue to its drive. The observation that it extends across the separatrix qualitatively supports its effect on transport. The radial width of the QCM remains a puzzle, with the optical diagnostics (GPI and BES) yielding a significantly larger width than the probe and reflectometer measurements. Although it is conceivable that the effective radial resolutions of the optical diagnostics are being increased in some unforeseen way (for example, in the GPI case by a larger toroidal extent of the gas-puff), the observed radial phase variation is not consistent with this kind of effect.

Blob generation and transport dynamics [18] are also not fully known. The in/out asymmetry is indicative of a ballooning-like drive [15]. The comparisons of blob characteristics in L- and H-Mode, both here and elsewhere [14,16], indicate that the blobs are not directly involved with the physics of the L-H transition, the pedestal formation or its sustainment. On the other hand the blob generation and transport do appear to play a role in density limit, with blob generation extending in to closed flux surfaces as the limit is approached.

Acknowledgement

Work supported at MIT by DoE Coop. Agreement DE-FC02-99ER54512, Contract No. DE-AC02-76CHO3073, and Grant DE-FG03-96ER54373.

References

-
- [1] B. LaBombard *et al.*, Phys. Plasmas **8** (2001) 2107.
 - [2] B. Carreras *et al.*, Physics of Plasmas **8** (2001) 3072.
 - [3] M. Umansky *et al.*, Phys. Plasmas **5** (1998) p 3373
 - [4] J.L. Terry *et al.*, J. Nucl. Mater. **290** (2001) 757.
 - [5] R. J. Maqueda *et al.*, Rev. Sci. Instrum. **72** (2001) 931.
 - [6] S. J. Zweben *et al.*, Phys. Plasmas **9** (2002) 1981.
 - [7] J.L. Terry *et al.*, Rev. Sci. Instrum. **75**, to appear in Oct (2004)
 - [8] A. Mazurenko *et al.* PRL **89** (2002) p 225004.
 - [9] B. LaBombard *et al.*, Nucl. Fus **40** (2000) 2041.
 - [10] A. E. Hubbard *et al.*, Phys. Plasmas **8** (2001) 2033.
 - [11] J. A. Snipes *et al.*, Plasma Phys. Controlled Fusion **43** (2001) L23.
 - [12] M. Sampsell, Ph.D. Thesis, U. of Texas at Austin, Dept. of Physics (pending 2004).
 - [13] J.W. Hughes *et al.* Phys. Plasmas **9** (2002) 3019.
 - [14] D.L. Rudakov *et al.*, Plasma Phys. Controlled Fusion **44** (2002) 717.
 - [15] J.L. Terry *et al.*, Phys. Plasmas **10** (2003) 1739.
 - [16] J.A. Boedo *et al.*, Phys. Plasmas **8** (2001) 4826.
 - [17] J.L. Terry *et al.*, to be published in J. Nucl. Mater. 2005.
 - [18] D.A. D'Ippolito and J.R. Myra, Phys. Plasmas **10** (2003) 4029.